ACS Catalysis

Research Article

pubs.acs.org/acscatalysis

Mechanism of Meropenem Hydrolysis by New Delhi Metallo β-Lactamase

Ravi Tripathi and Nisanth N. Nair*

Department of Chemistry, Indian Institute of Technology Kanpur, Kanpur 208016, India

Supporting Information

ABSTRACT: New Delhi metallo β-lactamase (NDM-1) is a recent addition to the metallo-β-lactamases family that is capable of hydrolyzing most of the available antibiotics, including the new generation carbapenems. Here, we report the mechanism of Meropenem hydrolysis catalyzed by NDM-1 based on hybrid quantum-mechanical/molecular-mechanical metadynamics simulations. Our work elicits the molecular details of the catalytic mechanism and free energy profiles along the reaction pathway. We identified the ring opening step involving the nucleophilic addition of the bridging hydroxyl group on the β-lactam ring of the drug as the rate-determining step. Subsequent protonation of β-lactam nitrogen occurs from a bulk water molecule that diffuses into the active site and is preferred over proton transfer from the bridging hydroxyl group or from the protonated Asp_{124}. The roles of important active site residues of NDM-1 and change in the coordination environment of Zn ions during the hydrolysis are also scrutinized.

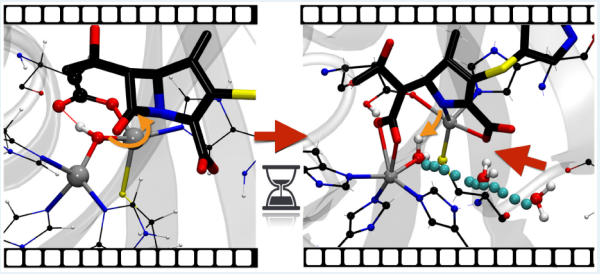

KEYWORDS: *NDM-1, β-lactamase, Meropenem, antibiotic resistance, QM/MM, molecular dynamics, hydrolysis, mechanism*

1. INTRODUCTION

Infections due to New Delhi metallo-β-lactamase (NDM-1) enzyme-carrying pathogens is a major concern for public health care today.[1,2] These pathogens show resistance to most of the β-lactam antibiotics, including the new generation carbapenems.[3] Resistance is achieved through expressing the NDM-1 enzyme, which can hydrolyze β-lactam antibiotics efficiently. Recent reports also indicate expressions of mutated NDMs (called NDM-2, 3, ..., 12) in bacteria as a part of their evolution toward achieving better antibiotic resistance.[4,5] Thus, it is imperative that we develop inhibitors for NDMs and also predict the potent mutations that the pathogens might adapt in the immediate future.

NDM-1 belongs to the metallo-β-lactamase (MBL) family[3,6,7] of β-lactam enzymes. Recent crystallographic[8,9] and spectroscopic studies[10] have confirmed that NDM-1 has two Zn ions bridged by a hydroxyl or a water molecule. Several crystal structures of NDM-1, in the apo form as well as in the complex forms with hydrolyzed drugs, are now available.[8,9,11−15] The active site of the enzyme has two Zn binding sites, Zn_1 and Zn_2. Zn_1 is coordinated to three histidines (His_{120}, His_{122}, and His_{189}), and the Zn_2 is ligated with Asp_{124}, Cys_{208}, and His_{250}. Many experimental and theoretical studies have also been carried out[3,8−10,14−22] to scrutinize the catalytic mechanism of NDM-1. The currently accepted general mechanism of hydrolysis,[7] is given in Figure 1.

The first step in the hydrolysis comprises a nucleophilic attack of the hydroxide (W1) bridging the two Zn ions to the β-lactam carbonyl carbon, assisted by the breaking of the C_4-N_2 bond.[6,7,23,24] The reaction proceeds via the intermediates **ES** (Michaelis complex), **EI** (ring-opened complex with lactam N bound to Zn_2), and **EP** (ring-opened complex with protonated lactam N).[10] It is now understood that in the di-Zn B1 type MBLs, Zn_1 has the role of stabilizing the negative charge developing on the carbonyl oxygen (O_3) during the nucleophilic attack of W1 (**ES** → **EI**).[8,23,25] Similarly, Zn_2 stabilizes the **EI** complex by coordinating with the negatively charged lactam nitrogen (N_2) after the scission of the C−N bond during the **ES** → **EI** reaction.[23] Zn_2 is also thought to be bound to the oxygen atoms (O_5,O_6) of the carboxyl group of the drug during its binding and the hydrolysis reaction.

The mechanism of protonation of N_2 is yet to be elucidated, and the controversy is mainly surrounding the source of the proton. Putative candidates for the proton donor are W1, Asp_{124}, and a bulk water molecule. W1 was suggested to be the proton donor by Zhang and Hao, on the basis of the distance between the oxygen of W1 and N_1 in the crystal structure of the **EI** complex formed by NDM-1 and ampicillin.[9] Asp_{124} in its protonated form is also capable of donating its proton to N_2.[26] Moreover, some of the NDM-1 X-ray structures[8,9] of **EI** complex also reveal the presence of a water molecule (presumably in the hydroxide form) between the Zn ions. This adds the possibility of protonation of N_2 by a bulk water molecule that diffuses to the active site of the **EI** complex.

Presteady state kinetic studies by a NDM-1 fused protein by Yang et al.[10] showed that the rate-determining step in the

Received: February 5, 2015
Revised: March 12, 2015
Published: March 13, 2015

DOI: 10.1021/acscatal.5b00242
ACS Catal. 2015, 5, 2577−2586

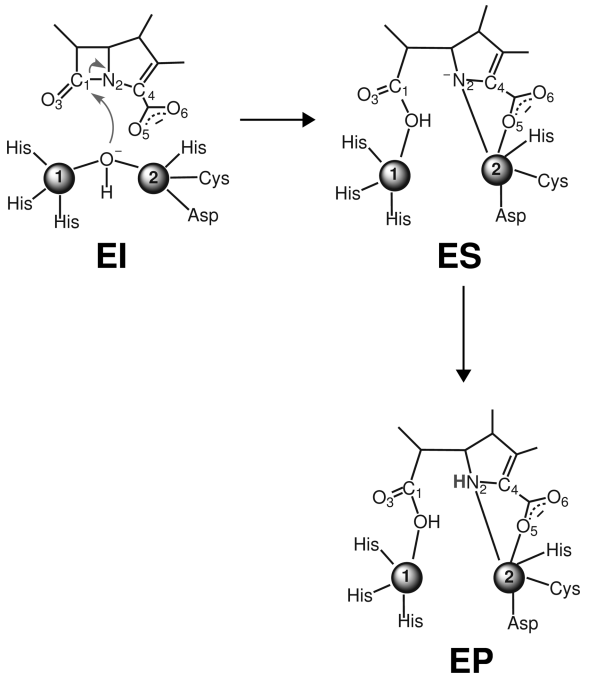

Figure 1. General mechanism for the hydrolysis of β-lactam antibiotic by NDM-1. Atoms with labels 1 and 2 are Zn_1 and Zn_2, respectively.

hydrolysis of nitrocefin and chromacef is the protonation of N_2. The same conclusion was also derived for other di-Zn MBLs using nitrocefin.[27−30] In the very recent kinetic and spectroscopic studies of the hydrolysis reaction of chromacef by dimetallic analogues of NDM-1, Yang et al.[19] arrived at the same conclusion regarding the rate-limiting step. However, in all these studies, the nitrocefin and chromacef were taken as the substrates. These are unusual antibiotics in which the anionic intermediate formed during the reaction can get stabilized by extended π delocalization.[31] A recent study reports that cephalosporin hydrolysis proceeds via tautomerization of the intermediate and concluded that the proton transfer step is the rate-determining step.[15] In kinetic studies performed with other substrates, the rate-determining step was proposed to be the cleavage of the β-lactam bond.[32,33] The extent of stabilization of the anionic intermediate may play a crucial role in the overall kinetics, which could vary among various classes of antibiotics.

Several computational studies have been carried out to understand the detailed hydrolysis mechanism of di-Zn MBLs.[34−36] Molecular simulations (MD), which is an ideal tool for obtaining the detailed dynamics during the hydrolysis of the drug, were employed for studying various MBLs.[34,36−38] In addition, a few theoretical studies have been devoted to the catalytic mechanism of NDM-1; however, they did not investigate beyond the nucleophilic attack step **ES→ EI**. In an in-depth study, Zhu et. al.[17] favored the deprotonated form of Asp_{124} during the ring-opening process of Meropenem in NDM-1. Among the various models considered in their study, they found that the one with the carboxylate group of the drug directly coordinated to Zn_2 and with Asp_{124} in its deprotonated state best represents the Michaelis complex of NDM-1 with Meropenem.

On the basis of the combined X-ray crystallographic study and QM/MM investigation, Joachimiak and co-workers[14] proposed a novel mechanism for the ampicillin hydrolysis in NDM-1. It was proposed that a bulk water molecule, after being activated by the embedded OH/water molecule, acts as a nucleophile in the first step of drug hydrolysis by NDM-1. The authors were able to see the entry of a monolayer of water molecules inside the active site of NDM-1 during 30 ns of their MD simulation. It was also shown that subsequent to the nucleophilic attack, another bulk water molecule abstracts a proton from W1 and transfers it to N_2. The possibility of W1 being the nucleophile was discarded by their study on the basis of the relatively high energy barrier obtained for this particular process.

In a recent study, Zheng et al.[18] investigated the ring opening step in ampicillin by NDM-1. They showed that the Michaelis complex of NDM-1 and drug does not involve coordination between the drug carboxylate and Zn_2. In accordance with previous studies on MBLs,[34,35] they also observed a proton transfer from W1 to Asp_{124} during the nucleophilic attack of W1. Although these studies are able to provide the detailed insights on the nucleophilic attack of a hydroxide to the carbonyl group and subsequent ring opening of the β-lactam ring of the drug molecule, the following step involving the protonation of N_2 remains elusive. Modeling of the complete reaction mechanism involving the nucleophilic attack and proton transfer step is thus vital to understanding the overall change in their coordination environment during the hydrolysis reaction and to identify the rate-determining step.

For simulating the hydrolysis reaction, it is vital to account for the dynamics of the solvated protein, specifically that of the active site residues. This is even more important for the Zn-based metallo proteins because of the flexible nature of the Zn ligand sphere.[6,7,22] Moreover, as a result of several plausible reaction routes, a simulation protocol[39] that is least biased by the chemical intuitions is preferred to model this enzymatic reaction. Thus, we carried out hybrid quantum chemical/molecular mechanical (QM/MM)[40,41] metadynamics[42,43] simulations to unveil the complete hydrolysis mechanism of Meropenem by NDM-1 (see Figure 3). This study provides profound insights at the molecular level on the hydrolysis reaction by NDM-1. These results could be used to understand the hydrolysis of other antibiotics by NDM-1 and other di-Zn B1MBLs.

2. METHODS AND MODELS

2.1. System Setup and Molecular Mechanics Simulation. The starting structure of the Henry−Michaelis complex of Meropenem and NDM-1 was modeled from the X-ray structure of NDM-1 in complex with the hydrolyzed Meropenem (PDB ID: 4EYL[8]); see also Figure 2. The lactam ring of Meropenem was first built using the molden software[44] and then optimized using the Gaussian 09 suite of programs[45] at the HF/6-31+G* level of theory. The initial structure was made with the deprotonated form of Asp_{124}. The system was

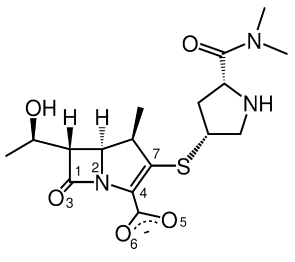

Figure 2. Structure of Meropenem.

DOI: 10.1021/acscatal.5b00242
ACS Catal. 2015, 5, 2577−2586

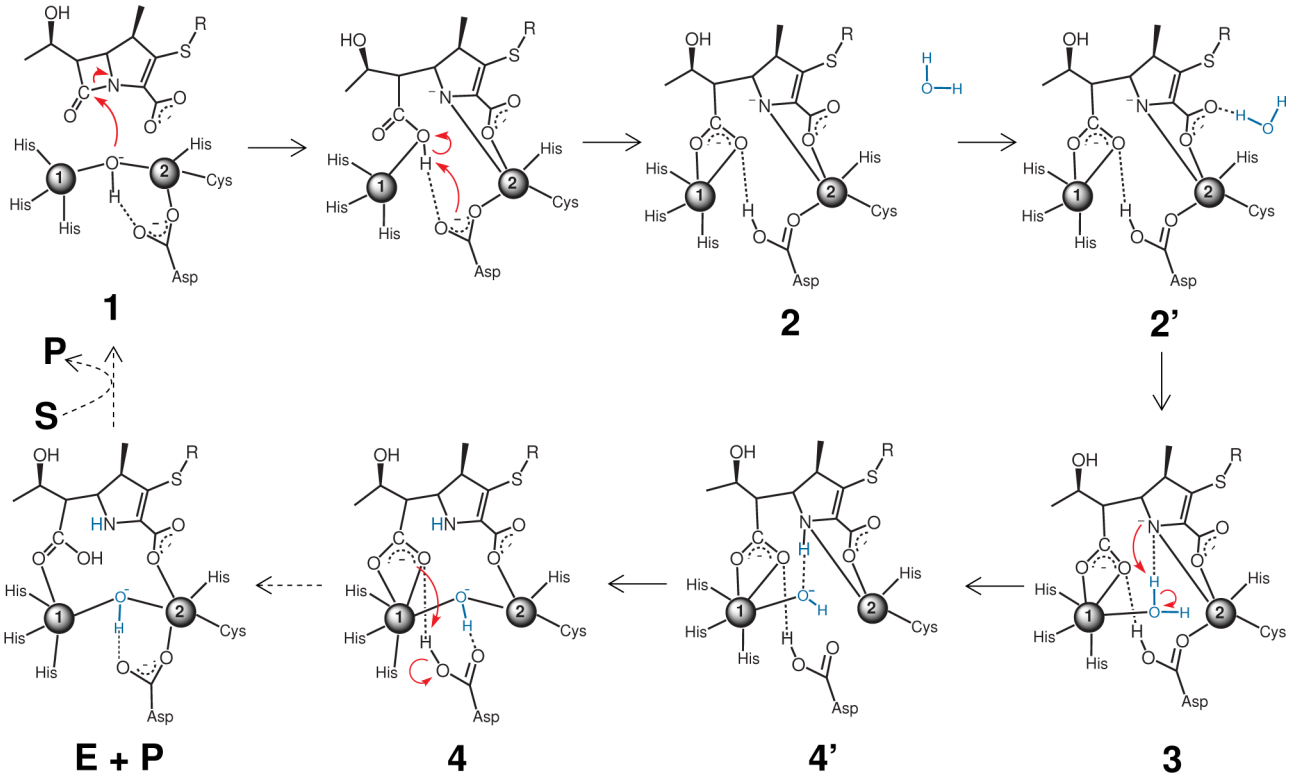

Figure 3. Observed mechanism of Meropenem hydrolysis by NDM-1. The dotted arrows are the hypothesized steps based on our simulation. In structures **2**, **2′**, and **3**, the negative charge on N_2 is delocalized over N_2−C_4 and C_4−C−7 bonds.

neutralized by adding Na^+ and Cl^- counterions and solvated with the TIP3P solvent model in a periodic box of dimension 67 × 65 × 68 Å^3. The parm99 version of the Amber force field[46] was used to describe the protein molecule, whereas the Meropenem molecule was treated using the GAFF force field.[47] Restrained electrostatic potential (RESP) charges of Meropenem were computed using the R.E.D. package.[48] The protonation states were set to that corresponding to pH = 7 for all the ionizable amino acid residues, except Asp_{124}. In accordance with ref 49, a bonded approach was adopted to maintain the coordination environment around Zn ions during MM MD simulations, which involves placing a harmonic bond between Zn ions and its surrounding residues. This included the covalent bonding interactions of Zn_1 with His_{120}, His_{122}, and His_{189}; and Zn_2 with Asp_{124}, Cys_{208}, and His_{250} (see Figure S1). Moreover, two additional bonds were defined between the Zn ions and the embedded hydroxide to maintain the "Zn_1−OH−Zn_2" bridged configuration.

The particle-mesh Ewald method was used to treat long-range interactions. A time step of 1 fs was chosen, and a nonbonded interaction cutoff of 15 Å was defined. Following the initial minimization, a 1 ns of *NPT* simulation was performed to equilibrate the density of the system. The pressure (1 atm) and temperature (300 K) were maintained using the Berendsen barostat and the Langevin thermostat, respectively. This was followed by a 5 ns of *NVT* simulation with the equilibrated cell volume obtained from the *NPT* simulation.

2.2. QM/MM Simulation. Hybrid QM/MM simulations[40] were performed using the CPMD/GROMOS interface,[50,51] as available in the CPMD package. The side chains of His_{120}, His_{122}, Asp_{124}, His_{189}, Cys_{208}, and His_{250} were treated using QM (see Figure S1). In addition to these, the whole Meropenem, the embedded hydroxide W1, and both Zn ions were included in the QM system. If a QM and an MM partition is defined between a chemical bond, the boundary atom is capped with hydrogen atoms. Capping hydrogen atoms were introduced between the C_β−C_γ bonds in His_{120}, His_{122}, His_{189}, and His_{250} and between the C_α−C_β bonds in Asp_{124} and Cys_{208}. The QM system was treated by density functional theory (DFT) using the PBE functional[52] and ultrasoft pseudopotentials.[53] The plane wave basis set with a plane wave cutoff of 25 Ry was used here. A total of 96 QM atoms were taken inside the QM box of dimension 27.5 × 27.5 × 22.7 Å^3. The electrostatic coupling between the QM and the MM subsystems was described using the scheme proposed by Liao et al.[50] The dynamics of the QM part was performed using the Car−Parrinello MD method.[41,54] The temperature of the system was maintained at 300 K using a Nosé−Hoover chain thermostat.[55] The fictitious mass of 700 au was assigned to the electronic orbital degrees of freedom, and a time step of 0.145 fs was used. Orbital degrees of freedom were thermostated using the Nosé−Hoover chain thermostats. the mass of a hydrogen atom was changed to that of the deuterium for maintaining adiabatic separation between nuclei and wavefunction degrees of freedom during the Car−Parrinello MD.

2.3. Metadynamics. On the basis of the previously reported studies and from experimentally known k_{cat} values, the typical timescale of the hydrolysis reactions by NDM-1 is of the order of seconds[3,10] at about 300 K. Since the time scale that can be accessed from the QM/MM MD simulations is limited to a few tens of picoseconds only, simulating this enzymatic reaction is beyond the scope of traditional QM-based MD simulations. Here, we employ the metadynamics[42,43] technique to overcome this time scale bottleneck in QM/MM MD simulations. For the details of the metadynamics

DOI: 10.1021/acscatal.5b00242
ACS Catal. 2015, 5, 2577−2586

technique, see reviews refs 56−59. In this method, a few coordinates, called collective coordinates (CCs) are chosen for their enhanced sampling. We employed the extended Lagrangian variant[43] of metadynamics in the current study, in which the extra degrees of freedoms, termed as collective variables (CVs), harmonically coupled to each CC are introduced. Bias potentials are added to enhance the dynamics of CVs, which in turn drive the CCs in the direction of chemical reactions due to the harmonic coupling between them. Technical details of the metadynamics simulations are identical to ref 60 CVs chosen for the current work, and related metadynamics parameters are given in the SI, Section 2. The free energy landscapes were obtained as the negative sum of the added biasing potentials. The mechanism and free energies are obtained from the reconstructed free energy landscapes. The committor probabilities of crucial transition state structure were computed for quantifying the accuracy of these structures; see SI, Section 3.1, for more details about these calculations. We also carried out convergence tests for the free energy barrier for the rate-determining step (see Section 3.1).

3. RESULTS

3.1. Equilibrium Structure of NDM-1/Meropenem Henry−Michaelis Complex. MM MD equilibration simulations were initially performed to obtain a starting structure for the QM/MM MD simulations. The root-mean-square deviation (RMSD) of the protein backbone with respect to the X-ray structure (PDB ID: 4EYL[8]) was calculated to monitor the structural changes during the simulation. Note that this X-ray structure has the **EI** complex with the hydrolyzed drug and is not in the precomplexed **ES** form; thus, the computed RMSD values may be considered with care. X-ray structures of **ES** complexes of NDM-1 are not available in the literature. The RMSD was found to be ∼1.5 Å; see Figure S3. In addition, the RMSD values of the active site of NDM-1 show a maximum deviation of only 1 Å (see Figure S4). These data provide confidence on the employed MM force field and the simulation protocols.

The active site of NDM-1 is largely composed of hydrophobic residues. Lys_{211} and Asn_{220} are the only active site residues that make hydrophilic interactions with the drug. We observed that the C_4 carboxylate group interacts with the side chains of Lys_{211} and Asn_{220}. The carboxylate group interacts with Lys_{211} and forms a hydrogen bond with the backbone NH group of Asn_{220} (see Figure 4 and Table 1). An additional hydrogen bond was formed between the side chain NH_2 group of Asn_{220} and carbonyl O_3 of the Meropenem. The average distance between Zn_1 and O_3 was measured at >3.3 Å, suggesting a weak interaction between them. Moreover, the distance of O_{W1} to the carbonyl C_1 (3.10 ± 0.14 Å) confirms that W1 is optimally positioned to make a nucleophilic attack on the carbonyl group of the drug molecule. The distance between Zn_1 and Zn_2 (3.35 ± 0.09 Å) is in close agreement with previous experimental studies on apo NDM-1.[10,11] In addition, this is in line with the previous computational studies of the **ES** complexes of NDM-1.[17,18] The interaction between the W1 proton and the carboxylate group of the Meropenem was observed during 86% of the *NVT* trajectory. Moreover, short-lived structures in which the W1 proton is hydrogen-bonded to the carboxylate group of the Asp_{124} were also observed during the simulation.

3.2. QM/MM Metadynamics Simulation of Meropenem Hydrolysis by NDM-1. *3.2.1. Step 1: Nucleophilic Attack.* A 6.8 ps of QM/MM simulation was performed starting with the final snapshot obtained from the MM MD simulation of NDM-1/Meropenem Michaelis complex. The starting structure had the W1 proton (H_{W1}) interacting with the Asp_{124} carboxylate group through a hydrogen bond. The interaction between the two remained stable during the QM/MM simulation. Moreover, the rest of the crucial interactions observed during the MM MD simulation (as discussed in the previous section) were also preserved during this simulation.

This was followed by a metadynamics simulation of the nucleophilic attack of W1 to C_1 in the **ES** complex (**1**; see also Figure 5). The following CVs were chosen to explore the mechanism of the nucleophilic attack: (a) coordination numbers of O_{W1} and C_1, minus coordination number of C_1 and N_2 (CV1); (b) coordination number of W1 to both the Zn ions (CV2); and (c) coordination number of N_2 to Zn_2 (CV3). CV1 was selected to accelerate the nucleophilic attack of W1 onto the carbonyl carbon of Meropenem and the breaking of the C−N bond of the lactam ring. CV2 was defined to sample the distance between W1 and both the Zn ions because breaking of the coordination interactions of W1 with the Zn ions is anticipated during the nucleophilic attack. CV3 was used to sample the distance between Zn_2 and N_2 because a bond formation between the two atoms is expected after the cleavage of the C−N bond of the β-lactam ring. Metadynamics simulation could successfully sample the nucleophilic attack

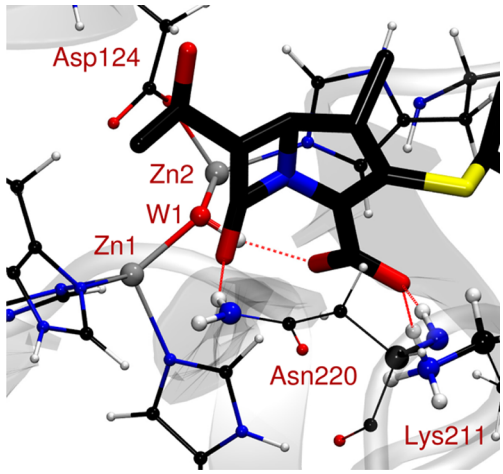

Figure 4. Equilibrated active site structure of NDM-1/Meropenem Michaelis complex; color code: Zn, gray; C, black; O, red; N, blue; S, yellow; and H, white. Active site residues and the drug molecule are in CPK and stick representations, respectively. Red thin lines show H bonds.

Table 1. Average Distance (in Å) between Selected Atoms in the Active Site of Equilibrium Structure Obtained from the MM MD Simulation[a]

atoms	distance
$O_{W1}\cdots C_1$	3.10 (±0.14)
$Zn_2\cdots O_5$	3.69 (±0.28)
$O_6\cdots Lys_{211}N_\zeta$	2.83 (±0.11)
$O_6\cdots Asn_{220}H$	2.01 (±0.19)
$O_3\cdots Zn_1$	3.35 (±0.21)
$O_3\cdots Asn_{220}N_\delta$	3.00 (±0.40)
$Zn_1\cdots Zn_2$	3.35 (±0.09)
$H_{W1}\cdots O_5$	2.08 (±0.26)

[a]Standard deviations are shown in brackets.

DOI: 10.1021/acscatal.5b00242
ACS Catal. 2015, 5, 2577−2586

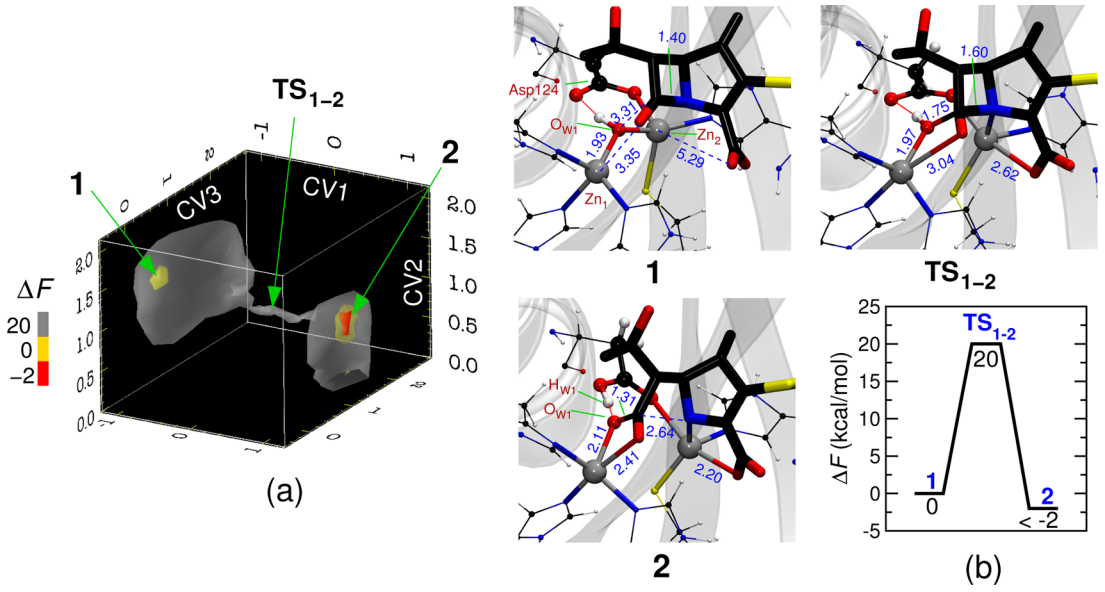

Figure 5. (a) Reconstructed free energy surface and the snapshots corresponding to structures **1**, $\mathbf{TS_{1-2}}$, and **2** from the metadynamics simulation of nucleophilic attack of W1 on C_1, in the NDM-1/Meropenem complex. Some of the crucial distances (in Å) are also indicated in the snapshots. For the minimum energy structures **1** and **2**, these distances were obtained from averaging 2 ps of QM/MM MD simulations. (b) Free energy profile for the reaction obtained by analyzing the free energy surface in part a.

of W1. We found that the reaction was leading to the formation of **2**, which is identical to the expected **EI** complex. The reconstructed free energy surface is shown in Figure 5. The reaction from **1** to **2** proceeds through the transition state structure $\mathbf{TS_{1-2}}$. The free energy barrier for the reaction **1** → **2** was found to be 20 kcal mol^{-1}. The simulation was continued until the product basin was filled up to 22 kcal mol^{-1}, which is sufficient to conclude that the reverse barrier for the nucleophilic attack, that is, for the process **2** → **1**, is higher than the forward barrier.

The nucleophilic attack by W1 on C_1 and the ring opening were found to be concerted (see Figure 6), and no stable intermediate structures were observed during this reaction. Interestingly, bonds between the carbonyl oxygen O_3 and Zn_1 and between the drug carboxylate group and Zn_2 were formed only when the system approached the transition state (see

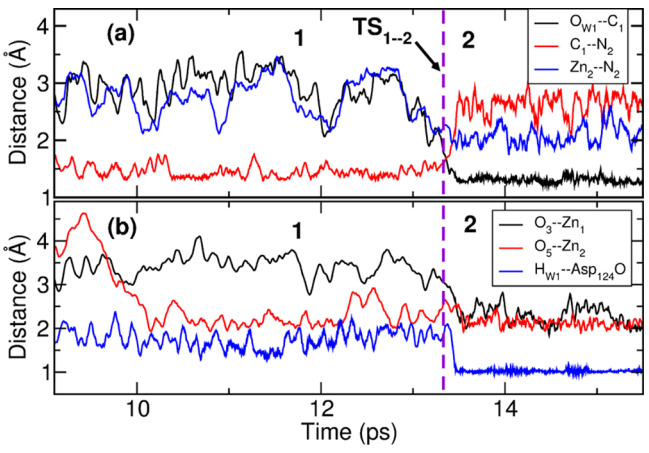

Figure 6. Plots of various distances during the metadynamics simulation of nucleophilic attack of W1 to C_1. The *X* axis shows the metadynamics time. The dotted vertical line indicates the position of $\mathbf{TS_{1-2}}$.

Figure 6). Here, the Zn_2 and W1 bond is broken during the reaction, while the former makes two new bonds with C_4 carboxylate and N_2. After the ring opening, the N_2 coordinates with Zn_2, stabilizing the negative charge developed on N_2 and the distance between them reduced to 2 Å. Zn_1 retains its coordination with W1 throughout the reaction but makes an additional (weak) bond with O_3 of the carbonyl group while forming $\mathbf{TS_{1-2}}$ ($d[Zn_1{-}O_3]$ = 3.05 Å). Thus, the coordination of both the Zn ions was increased from 4 to 5 in going from **1** to **2**. Interestingly, a proton transfer from W1 to one of the carboxylate O atoms of Asp_{124} was preceded by the nucleophilic attack. The mechanism of **1** → **2**, as obtained from this simulation, is shown in Figure 3. A movie file (Movie_1–2.mpg) showing the reactive trajectory **1** → **2** is available in the SI for further reference.

To achieve confidence on the saddle point structure obtained from the metadynamics simulation, we computed the committor probability for the $\mathbf{TS_{1-2}}$ structure, as explained in SI, Section 3.1. The committor probabilities of 57% to **1** and 43% to **2** were obtained, which indicate that $\mathbf{TS_{1-2}}$ is very close to the actual transition state structure.

3.2.2. Step 2: Proton Transfer. The second step in the drug hydrolysis by NDM-1 is the protonation of N_2. The exact mechanism of the protonation of N_2, especially the identity of the proton donor, has been highly contentious. Various proposals have been put forth regarding the source of proton, as discussed in the Introduction. One of the proposals is by Zhang and Hao.[9] Their proposal that the proton is transferred from W1 to N_2 is based on the close distance between the two in the X-ray structure of NDM-1 complexed with hydrolyzed ampicillin (PDB ID: 3Q6X). To validate this possibility, we carried out a metadynamics simulation starting with the ring-opened structure **2** obtained from the previous metadynamics simulation. It may be noted that O_{W1} is deprotonated in **2**, and the H_{W1} is bound to the carboxylate group of Asp_{124}. The following CVs were chosen for this study: (a) coordination number of both $Asp_{124}O$ atoms and H_{W1} minus the

DOI: 10.1021/acscatal.5b00242
ACS Catal. 2015, 5, 2577–2586

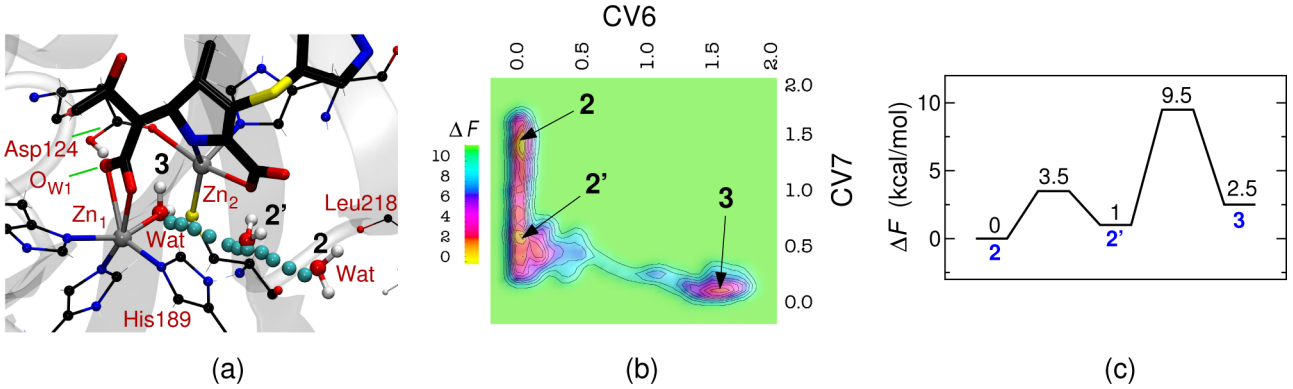

Figure 7. (a) Structure of **3**, together with the path that the bulk water Wat has taken to enter the active site of NDM-1 (cyan spheres); the Wat molecule in **2** and in an intermediate structure **2′** are also shown, together with the active site structure of **3**. (b) Free energy surface and (c) free energy profile for **2** → **3**.

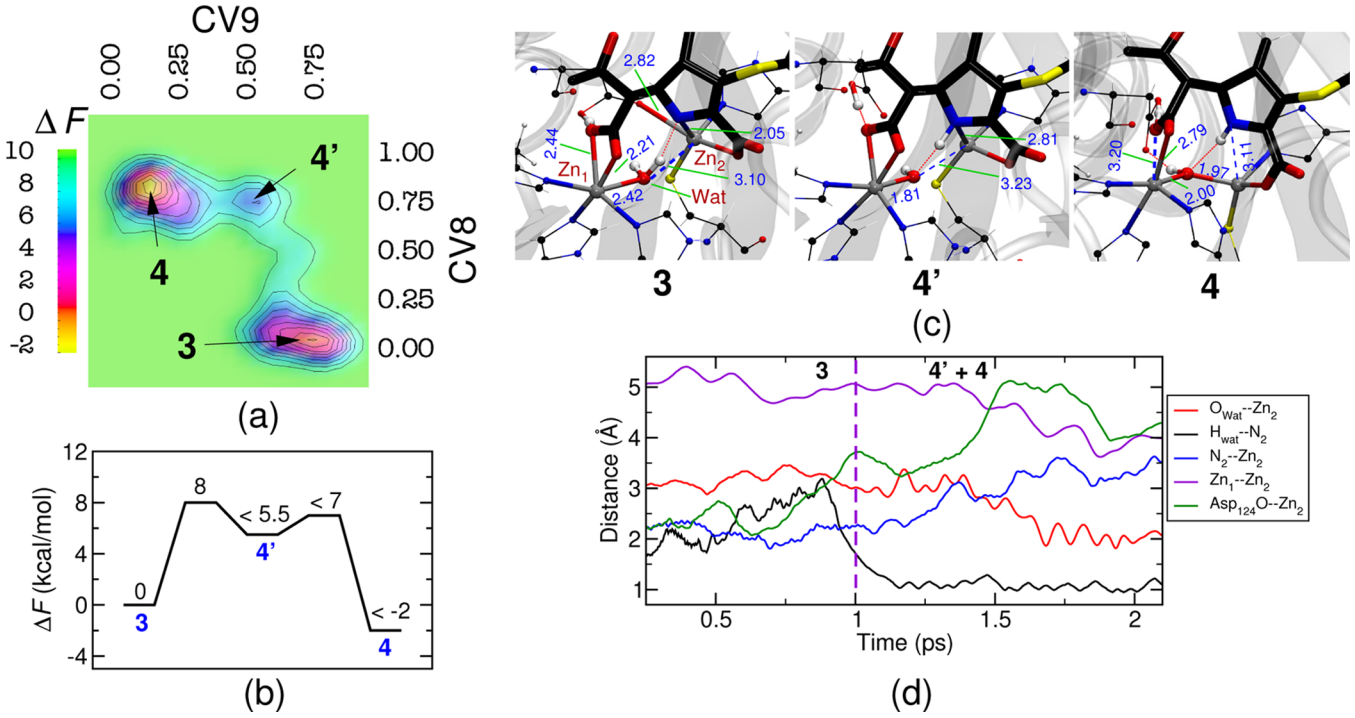

Figure 8. (a) Free energy surface, (b) free energy profile, (c) representative snapshots for **3** → **4** reaction. In part d, crucial distances during the metadynamics simulation are shown. The dotted vertical line is shown to differentiate the domains for **3** and **4′** + **4**.

coordination number of O_{W1} and H_{W1} (CV4); (b) the coordination number of H_{W1} and N_2 (CV5). CV4 was chosen to sample the H_{W1} transfer between O_{W1} and $Asp_{124}O$. This is to account for the possibilities of proton transfer to N_2 either directly from $Asp_{124}O$, or from O_{W1}. CV5 was selected to accelerate the proton transfer of H_{W1} to N_2. The reconstructed free energy surface is shown in Figure S5. An intermittent proton transfer from $Asp_{124}O$ to O_{W1} was seen, although the proton remained largely with Asp_{124}. This is also clear from the free energy surface, where no minimum can be found in the negative values of CV4, although such values of this CV were sampled. Thus, we can conclude that there is no reverse barrier for the H_{W1} transfer from O_{W1} to $Asp_{124}O$. Moreover, the proton transfer to N_2 did not occur, even when the free energy well was filled up to 24 kcal mol^{-1}. This indicated to us that a direct protonation of N_2 from O_{W1} or Asp_{124} may not be the actual mechanism that is followed by these enzymes.

3.2.3. Bulk Water Entry to the Active Site. On closer inspection of the active site of **2**, we found the presence of water molecules within 7 Å of the Zn ions. Two X-ray structures of NDM-1 bound to the ring-opened drug molecule[8,9] have a water molecule or a hydroxide ion bridging between the two Zn ions. On the basis of the distance between the Zn ions in these structures (≈4.5 Å), we interpret that the water molecule is in the molecular form, not in the hydroxide form. The distance between the Zn ions that are bridged by a hydroxide was found to be ∼3.5 Å in the previous computational studies of the **ES** complex of NDM-1.[17,18] The presence of a water molecule between the two Zn ions in the **EI** complex suggests that a water molecule from the bulk enters the active site before the exit of the hydrolyzed drug. This has motivated us to look at an alternative mechanism for proton transfer to N_2 where a water molecule from the bulk enters the

DOI: 10.1021/acscatal.5b00242
ACS Catal. 2015, 5, 2577−2586

active site of NDM-1 after the formation of **2** and donates its proton to N_2 forming **3** (see Figure 3).

Metadynamics simulations were carried out to validate this mechanism. Among several water molecules present in the vicinity of the Zn ions in **2**, one of them (Wat) was located in close proximity to the Leu_{218}, His_{189}, and carboxylate group of the drug and is suitably positioned to diffuse toward the interior of the active site. We carried out a metadynamics simulation to model the movement of Wat toward the active site. In this QM/MM simulation, the Wat molecule was modeled by the TIP3P force field and was not part of the QM region. CVs selected for the metadynamics simulation were (a) the coordination number of O_{Wat} to both the Zn ions (CV6) and (b) the coordination number of O_{Wat} to $Leu_{218}O$, $His_{189}H_{\delta}$, O_5, and O_6 (CV7). CV6 was selected to sample the distance of Wat to both the Zn ions, whereas CV7 was defined to accelerate the breaking of hydrogen bonding interactions of Wat with its surrounding residues. The reconstructed free energy profile is shown in Figure 7. We found that Wat approached the active site of NDM-1 crossing a free energy barrier of 9.5 kcal mol^{-1}. Water diffusion into the active site occurs in two steps: (a) the first step involves crossing a free energy barrier of 3.5 kcal mol^{-1}, forming an intermediate, **2′**, where Wat is ∼4.8 Å from Zn_1; (b) in the second step, the water molecule overcomes a barrier of 8.5 kcal mol^{-1} to form **3**. Wat was involved in hydrogen bonding interactions with $Leu_{218}O$ and $His_{189}H_{\delta}$in **2**. These interactions were broken during **2** → **2′**, but it formed O_5/O_6 interactions. Subsequently, the later interactions were lost on formation of the coordination bonds with Zn ions in **3** during **2′** → **3**. In **3**, Wat occupies the position between the two Zn ions without perturbing the crucial interactions existing in the active site. Wat is more strongly coordinated to Zn_1 than Zn_2, with Zn_1-O_{Wat} and Zn_2-O_{Wat} distances of ∼2.4 and 3.1 Å, respectively. A transient proton transfer between Asp_{124} and O_{W1} was, however, observed following the Wat insertion. A movie (Movie_2−3.mpg) showing the reactive trajectory **2** → **3** is available in the SI.

3.2.4. Proton Transfer from Wat to N_2. In **3**, the Wat is embedded between the two Zn ions and well oriented and positioned to provide its proton to N_2. To model the proton transfer from Wat to N_2, we performed a metadynamics simulation starting with **3**, the structure obtained from the previous metadynamics simulation. The Wat molecule is now included in the QM part of the simulation. Two CVs were defined for the metadynamics simulation: (a) coordination number of N_2 and the protons of W1 and Wat (CV8) and (b) the coordination number of N_2 and Zn_2 (CV9). CV8 was selected to accelerate proton transfer from W1/Wat to N_2, and CV9 was chosen for sampling the distance between N_2 and Zn_2.

We observed the proton transfer from Wat to N_2 in this simulation, and the mechanism is shown in Figure 3. The reconstructed free energy surface is shown in Figure 8, and three free energy minima can be identified here. Proton transfer from Wat to N_2 leads to **3** → **4′**. The free energy barrier for this process is ∼8 kcal mol^{-1}. Subsequently, **4** was formed from **4′** by the breakage of the Zn_2-N_2 bond and the formation of a Zn_2-O_{Wat} bond. The free energy barrier for **4′** → **4** was calculated to be 1.5 kcal mol^{-1}. Upon completion of the proton transfer reaction, the distance between the Zn ions changed from 5.1 to 3.8 Å (see Figure 8). W1 lost its coordination with Zn_1, and the deprotonated Wat established a coordination bond with both Zn ions in **4** (see Figure 8). Interestingly, the coordination between Zn_2 and Asp_{124} was completely lost when **4′** and **4** were formed. Going from **3** to **4**, the coordination numbers of Zn_1 and Zn_2 change from 6 to 5 and from 5 to 4, respectively.

A transient proton transfer from the protonated Asp_{124} carboxylate group to O_{W1}, which in these structures is a part of the carboxylate group of the drug bound to Zn_1, was observed during the simulation, although this proton remained largely with Asp_{124}. In fact, the proton transfer from Asp_{124} back to O_{W1} is expected during the final exit of the hydrolyzed Meropenem from the active site of NDM-1. This would re-form the apo structure of NDM-1 and completes the catalytic cycle (see also Figure 3). A movie file (Movie_3-4.mpg) showing the trajectory for the reaction **3**→ **4** is available in the SI.

4. DISCUSSION

4.1. Crucial Interactions in the Michaelis Complex and Their Relevance. In the equilibrated structure of **1** (**ES**) in the ASP-COO protonation state, a direct contact between O_5/O_6 carboxylate oxygens (of C_4) and Zn_2 was not observed. We found that the coordination between them is formed only when the system forms $\mathbf{TS_{1-2}}$ during the reaction **1**(**ES**) → **2**(**EI**) and remains associated until the formation of **4** (**EP**). This is different from the previous studies[17,34,35] on MBLs and NDM-1 in which Zn_2 was proposed to be penta-coordinated in the **ES** complex and is bound with carboxylate oxygens O_5/O_6. However, the recent study by Zheng and Xu[18] reveals that the interaction between O_5/O_6 and Zn_2 is formed only during the nucleophilic attack of W1 and not in the Michaelis complex, in agreement with our observations. No high-resolution crystal structure of the NDM-1/drug Michaelis complex is available to justify the presence of this bond in the **ES** complex. However, O_5/O_6 was found to coordinate Zn_2 in the crystal structures of NDM-1 complexed with the hydrolyzed drug molecules,[8,9] which is again in agreement with our computations. The coordination between Zn_2 and O_5/O_6 carboxylate is an essential feature of the transition state structure rather than the Michaelis complex. The importance of this interaction was perceived as providing a suitable orientation to the incoming drug for the hydrolysis.[61−63]

Earlier studies[64,65] on MBLs suggested that Zn_1 together with an active site residue forms an oxyanion hole interacting with the carbonyl group of the lactam ring during the nucleophilic attack. We found that the carbonyl group of Meropenem interacts mostly with the side chain of Asn_{220} in the **ES** complex. The average distance between O_3 and Zn_1 was calculated to be more than 3.3 Å in our MD simulations. Interestingly, the interaction between them was established once the transition state was approached (see $\mathbf{TS_{1-2}}$ and Figure 5), which then remained in the **EP** complex (**4**). This indicates that the Asn_{220} alone provides the oxyanion hole in NDM-1, whereas it employs Zn_1 in the transition state for the stabilization of the partial negative charge developed on the carbonyl O_3. This is in agreement with the computational study performed by Zheng and Xu[18] in which a similar role of Asn_{220} and Zn_1 was observed. See SI Section 7 for discussion on other interactions of the drug molecule with Lys_{211} and Asn_{220}.

4.2. Reaction Mechanism of Meropenem Hydrolysis. The reaction mechanism of Meropenem hydrolysis catalyzed by NDM-1 is shown in Figure 3. The first step of hydrolysis comprises nucleophilic attack by W1 on C_1 combined with the cleavage of the C−N bond of the β-lactam ring. Subsequently, Zn_2 stabilizes the negative charge developed on N_2 after the

DOI: 10.1021/acscatal.5b00242
ACS Catal. 2015, 5, 2577−2586

ring-opening process. This is consistent with the previous computational studies on NDM-1 and other MBLs.[17,18,34−36,66] In addition, a coordination bond between Zn_2 and N_2 is seen in several X-ray structures of NDM-1/MBLs bound to the ring-opened drug.[8,9,67]

A proton transfer from W1 to Asp_{124} takes place, preceded by the formation of the covalent bond between C_1 and W1 (see Figure 3). This is followed by the entry of a bulk water molecule into the active site of the **EI** complex (or **2**), which occupies the previous position of W1 bridging the two Zn ions. In the final step, proton transfer from this water to N_2 occurs, thus completing the hydrolysis of the drug molecule. The mechanism of protonation of N_2 is highly debated in the literature, and various proposals have been put forward regarding the source of the proton. A direct transfer of H_{W1} from Asp_{124} to N_2 in **3** is less probable because it requires breaking the hydrogen bond between $Asp_{124}H_{W1}$ and O_{W1} as well as the rotation of the Asp_{124} carboxylate oxygen atoms, which involves breaking the $Zn_2-Asp_{124}O$ bond. As a result, a direct proton transfer to N_2 from Asp_{124} becomes less favorable. The complete free energy profile for the Meropenem hydrolysis is shown in Figure 9. A trapped water molecule between the Zn

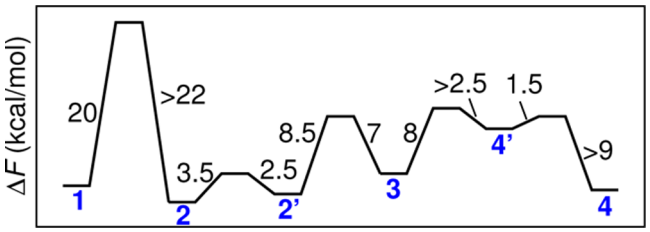

Figure 9. Free energy profile for the Meropenem hydrolysis catalyzed by NDM-1.

ions has been observed in many crystal structures of **EI** complexes of MBLs, including NDM-1.[8,9,67] The observed mechanism is in agreement with that proposed by Zhang and Hao.[9] A few of the earlier studies[27,31] have also hypothesized that bulk water can be a source of the proton during the protonation of N_2. Protonation of lactam nitrogen by an active site water molecule was also suggested in monozinc MBLs.[66]

We believe that the catalytic centers may reform by the detachment of the hydrolyzed Meropenem through the path **4** → **E** + **P**, as shown in Figure 3. Because the proton of W1 was transferred to Asp_{124} during the nucleophilic attack, a proton transfer from Asp_{124} back to W1 is expected during the exit of the hydrolyzed Meropenem from the active site of NDM-1. A transient proton transfer from $Asp_{124}O$ to O_{W1} was seen in the 4.3 ps of the QM/MM simulation performed with **4** (data not shown), which further strengthens this hypothesis.

In an earlier work by Kim et al.,[14] the full reaction mechanism was studied using static QM/MM methods. These authors proposed a mechanism in which a water molecule attacks on C_1 instead of W1, and subsequent proton transfer to N_2 from W1 occurs via another water molecule at the active site. However, the computed potential energy barrier for the nucleophilic attack of W1 was unrealistic (more than 41 kcal mol^{-1}), and thus, that mechanism can be ruled out.

4.3. Rate-Determining Step and Kinetics. The precise knowledge of the rate-determining step in the drug hydrolysis catalyzed by NDM-1 is still not established and warrants discussion. Our study using Meropenem shows that the rate-limiting step of the Meropenem hydrolysis by NDM-1 is the nucleophilic attack of the bridging hydroxide group on C_1 of the β-lactam ring and the concomitant ring opening by the C−N bond cleavage. Proton transfer to N_2 is not the rate-determining step.

In a recent study, by analyzing a series of NMR and EXAFS data together with steady-state and stopped-flow kinetics studies, Yang et al.[19] proposed that protonation of N_2 is the rate-limiting step in the chromacef hydrolysis by NDM-1. The same conclusion was also made for other MBLs, including NDM-1, on the basis of the observation of an accumulated intermediate corresponding to the ring-opened substrate during the nitrocefin and chromacef hydrolysis.[10,27−30] However, these studies used either nitrocefin or chromacef as the substrate for the spectroscopic and kinetic studies. The anionic intermediates formed by these molecules are particularly stable because of the extended π delocalization.[31,32] In contrast, a study of nitrocefin hydrolysis catalyzed by dinuclear Zn complexes shows that the rate-limiting step is the intramolecular attack by the bridging hydroxide, which is then followed by a fast protonation of the intermediate.[61] Walsh and co-workers[32] also detected distinct absorbance spectra for the nitrocefin intermediate during their experiments in L1 enzyme. However, in the same study using some other substrates, intermediates were detected with an intact β-lactam ring, which led them to conclude that the rate-limiting step for majority of the antibiotics is the breaking of the C−N bond in the lactam ring. These observations are in line with our findings.

Later, Rasia and Vila[33] carried out a pre-steady-state kinetics study of several drug molecules in the BcII enzyme but could not detect any chemically modified substrate species accumulating as the intermediate, which is again in agreement with our results. A recently published work by Feng et al.[15] has reported the X-ray structures of intermediates during the hydrolysis of some cephalosporin drug molecules by NDM-1. In these structures, they clearly noted the existence of an intermediate that has undergone a tautomerization after ring-opening, but not protonated. This led them to conclude that the rate-determining step is the protonation step. On analysis of structures **1**−**4**, we also observe charge delocalization between N_2, C_4, and C_7 in the intermediates **2**−**4**, as evident from their N_2-C_4, C_4-C_7 bond distances (see SI, Section 6). However, a protonation of C_7 is less likely in **2** or **3**, on the basis of the distance of the C_7 from the plausible proton donors. It is not clear if cephalosporin drug molecules behave differently from Meropenem (which belongs to the carbapenem family) in this respect.

The k_{cat} value of the Meropenem hydrolysis reaction by NDM-1 was reported to be 12 s^{-1} (at 30 °C),[3] implying that the free energy barrier for the reaction is ≈16 kcal mol^{-1}, using transition state theory. Thus, the computed free energy barrier (20 kcal mol^{-1}) is only 4 kcal mol^{-1} higher than this estimate. This discrepancy could be mostly due to the error in the PBE density functional, which is ∼2 kcal mol^{-1}, as discussed in SI, Section 3.1. On the basis of the results of our "shooting" simulations and metadynamics refinement runs (SI, Section 3.1), we believe that this difference cannot be due to the missing CVs and sampling/convergence problems of metadynamics.

4.4. Intermediate(s) during the Reaction. Our study shows that there are four intermediates during the course of the Meropenem hydrolysis. The two stable intermediates, **2** and **3**, have a free energy barrier of at least 8 kcal mol^{-1} for their decay

DOI: 10.1021/acscatal.5b00242
ACS Catal. 2015, 5, 2577−2586

and are likely to be trapped in the experiments at low temperatures. The two stable intermediates differ in the presence of a bulk water between the Zn ions. During the reaction **1** → **2** → **3** → **4**, the coordination numbers of Zn_1 and Zn_2 vary as 4 → 5 → 6 → 5 and 4 → 5 → 5 → 4, respectively. A significant structural similarity is noticed between the X-ray structures of NDM-1 in complex with ring-opened oxacillin[8] and the structure **3** (**EI**) obtained from our simulation (see Figure 10). The presence of multiple intermediates is also in accordance with the experimental observations of Vila and co-workers[68] for Co(II)-substituted BcII.

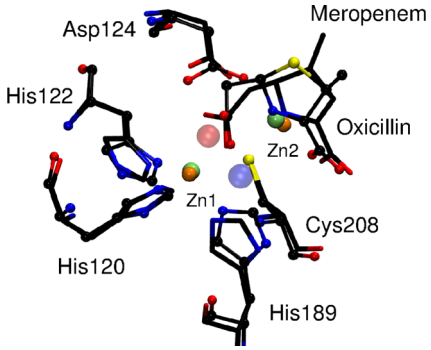

Figure 10. Structural superimposition of X-ray structure (PDB ID: 4EYB) (A)[8] (in CPK) with the ensemble average of the active site structure of **EI** complex **3** (in stick model) from QM/MM MD simulations. Only the β-lactam ring, the fused five-membered ring, and the carboxylate group of the drug molecules are highlighted. His_{250} is not shown here for more clarity. Zinc ions from simulation and X-ray are shown with orange and lime, respectively. The water molecule bridging the Zn ions in X-ray (red, big sphere and transparent) and **3** from our simulation (blue, big sphere and transparent) is also shown.

5. SUMMARY AND CONCLUSION

Using molecular dynamics simulations, we have reported here the molecular level details of the hydrolysis of Meropenem by NDM-1. During the nucleophilic attack of the bridging hydroxyl group, the β-lactam ring opening reaction occurs simultaneously with the formation of a bond between the β-lactam nitrogen (N_2) and Zn_2. Our simulations show that the carboxylate group of the Asp_{124} abstracts the proton of the hydroxyl group during the nucleophilic attack in a nearly concerted manner. A direct proton transfer from the bridging hydroxide group or from the protonated carboxylate group of Asp_{124} to the β-lactam nitrogen (N_2) in the **EI** complex is less likely. It was observed that diffusion of a bulk water molecule to the active site is a relatively fast process, which then bridges the two Zn ions and subsequently acts as the source of the proton for the subsequent protonation of N_2. By constructing the free energy profile for the entire hydrolysis reaction, it was observed that the rate-determining step is the nucleophilic attack of the bridging hydroxyl group, and the free energy barrier is ~20 kcal mol^{-1}. We found a striking similarity between the structures of the **EI** complex from X-ray and from our simulations. The hydrolysis of Meropenem occurs in a stepwise manner (Figure 3), with two stable intermediates of a lifetime corresponding to a free energy barrier of about 8 kcal mol^{-1}. These intermediates differ in the coordination sphere of Zn_1 and Zn_2 and may be traced in the experiments at low temperatures. Tautomerization of the double bond within the five-membered ring was not observed after the β-lactam ring opening, although the negative charge on N_2 is delocalized. During the hydrolysis reaction **1** → **2** → **3** → **4**, the coordination numbers of Zn_1 and Zn_2 change as 4 → 5 → 6 → 5 and 4 → 5 → 5 → 4, respectively.

The importance of the protein−drug interactions and the role of the key active site residues during the drug hydrolysis have also been scrutinized. Zn_1 was found to stabilize the transition state connecting **ES** and **EI** complexes, whereas the role of Zn_2 was seen in stabilizing the negative charge developed on N_2 after the β-lactam ring opening. Coordination of Zn_1 to the carbonyl oxygen of the β-lactam ring is not present in the Michaelis complex, but it is formed in the transition state connecting the **ES** and the **EI** complexes. The same is the case for Zn_2 and the drug carboxylate O_5/O_6 interactions. The other active site residues, such as Lys_{211} and Asn_{220}, also play a major role in suitably orienting the drug molecule at the active site. The bridging hydroxyl group and carboxylate of Asp_{124} interaction was present during the nucleophilic attack, on the basis of which we conclude that Asp_{124} is helping to position the bridging hydroxyl group in a favorable orientation for the reaction.

We believe that these results are useful for interpreting spectroscopic data, crystal structures, and kinetic experiments of Meropenem hydrolysis. Further, the wealth of molecular level details obtained in this study can expedite the development of new inhibitors and modified drugs to combat the outgrowing danger of NDM-1. To aid future research in this direction, we have deposited the coordinates of the intermediates and movies showing the elementary reactions in the Supporting Information.

■ ASSOCIATED CONTENT

Supporting Information

The following files are available free of charge on the ACS Publications website at DOI: 10.1021/acscatal.5b00242.

PDB files for the average structures **1** to **4** (ZIP)
Movies of the reactive trajectories for all the reactions studied here (.mpg files) (ZIP)
Various supporting data (PDF)

■ AUTHOR INFORMATION

Corresponding Author

*E-mail: nnair@iitk.ac.in.

Notes

The authors declare no competing financial interest.

■ ACKNOWLEDGMENTS

All the computations were performed at the HPC facility at IIT Kanpur. R.T. acknowledges the Council of Scientific and Industrial Research (CSIR), India, for a fellowship.

■ REFERENCES

(1) WHO; *Antimicrobial Resistance: Global Report on Surveillance 2014*; WHO Press, World Health Organization: Geneva, 2014.
(2) Bushnell, G.; Mitrani-Gold, F.; Mundy, L. M. *Int. J. Infect. Dis.* **2013**, *17*, e325−e333.
(3) Yong, D.; Toleman, M. A.; Giske, C. G.; Cho, H. S.; Sundman, K.; Lee, K.; Walsh, T. R. *Antimicrob. Agents Chemother.* **2009**, *53*, 5046−5054.
(4) Nordmann, P.; Poirel, L.; Walsh, T. R.; Livermore, D. M. *Trends Microbiol.* **2011**, *19*, 588−595.
(5) Tada, T.; Shresthac, B.; Miyoshi-Akiyamaa, T.; Shimadaa, K.; Oharab, H.; Kirikaea, T.; Pokhrelc, B. M. *Antimicrob. Agents Chemother.* **2014**, *58*, 6302−6305.

DOI: 10.1021/acscatal.5b00242
ACS Catal. 2015, 5, 2577−2586

(6) Umayal, M., Tamilselvi, A., Mugesh, G. *Prog. Inorg. Chem.*; 2012;57395−443.
(7) Palzkill, T. *Ann. N.Y. Acad. Sci.* **2013**, *1277*, 91−104.
(8) King, D. T.; Worrall, L. J.; Gruninger, R.; Strynadka, N. J. *J. Am. Chem. Soc.* **2012**, *134*, 11362.
(9) Zhang, H.; Hao, Q. *FASEB J.* **2011**, *25*, 2574−2582.
(10) Yang, H.; Aitha, M.; Hetrick, A. M.; Richmond, T. K.; Tierney, D. L.; Crowder, M. W. *Biochemistry* **2012**, *51*, 3839−3847.
(11) Guo, Y.; Wang, J.; Niu, G. J.; Shui, W. Q.; Sun, Y. N.; Lou, Z. Y.; Rao, Z. H. *Protein Cell* **2011**, *2*, 384.
(12) Green, V. L.; Verma, A.; Owens, R. J.; Phillips, S. E. V.; Carr, S. B. *Acta Crystallogr., F* **2011**, *67*, 1160.
(13) King, D.; Strynadka, N. *Protein Sci.* **2011**, *20*, 1484.
(14) Kim, Y.; Cunningham, M. A.; Mire, J.; Tesar, C.; Sacchettini, J.; Joachimiak, A. *FASEB J.* **2013**, *27*, 1917−1927.
(15) Feng, H.; Ding, J.; Zhu, D.; Liu, X.; Xu, X.; Zhang, Y.; Zang, S.; Wang, D.-C.; Liu, W. *J. Am. Chem. Soc.* **2014**, *136*, 14694−14697.
(16) Thomas, P. W.; Zheng, M.; Wu, S.; Guo, H.; Liu, D.; Xu, D.; Fast, W. *Biochemistry* **2011**, *50*, 10102.
(17) Zhu, K.; Lu, J.; Liang, Z.; Kong, X.; Ye, F.; Jin, L.; Geng, H.; Chen, Y.; Zheng, M.; Jiang, H.; Li, J.; Luo, C. *J. Comput.-Aided Mol. Res.* **2013**, *27*, 247−256.
(18) Zheng, M.; Xu, D. *J. Phys. Chem. B* **2013**, *117*, 11596−11607.
(19) Yang, H.; Aitha, M.; Marts, A. R.; Hetrick, A.; Bennett, B.; Crowder, M. W.; Tierney, D. L. *J. Am. Chem. Soc.* **2014**, *136*, 7273−7285.
(20) Poeylaut-Palena, A. A.; Tomatis, P. E.; Karsisiotis, A. I.; Damblon, C.; Mata, E. G.; Vila, A. J. *Bioorg. Med. Chem. Lett.* **2007**, *17*, 5171−5174.
(21) Yuan, Q.; He, L.; Ke, H. *Antimicrob. Agents Chemother.* **2012**, *56*, 5157−5163.
(22) Rydzik, A. M.; Brem, J.; van Berkel, S. S.; Pfeffer, I.; Makena, A.; Claridge, T. D. W.; Schofield, C. J. *Angew. Chem., Int. Ed.* **2014**, *53*, 3129−3133.
(23) Page, M. I.; Badarau, A. *Bioinorg. Chem. Appl.* **2008**, 17986−17988.
(24) Wang, Z.; Fast, W.; Valentine, A. M.; Benkovic, S. J. *Curr. Opin. Chem. Biol.* **1999**, *3*, 614−622.
(25) Crowder, M. W.; Spencer, J.; Vila, A. J. *Acc. Chem. Res.* **2006**, *39*, 721−728.
(26) Crisp, J.; Conners, R.; Garrity, J. D.; Carenbauer, A. L.; Crowder, M. W.; Spencer, J. *Biochemistry* **2007**, *46*, 10664−10674.
(27) Hu, Z.; Periyannan, G.; Bennett, B.; Crowder, M. W. *J. Am. Chem. Soc.* **2008**, *130*, 14207−14216.
(28) Wang, Z.; Fast, W.; Benkovic, S. J. *J. Am. Chem. Soc.* **1998**, *120*, 10788−10789.
(29) McManus-Munoz, S.; Crowder, M. W. *Biochemistry* **1999**, *38*, 1547−1553.
(30) Lisa, M. N.; Hemmingsen, L.; Vila, A. J. *J. Biol. Chem.* **2010**, *285*, 4570−4577.
(31) Karsisiotis, A. I.; Damblon, C. F.; Roberts, G. C. *Metallomics* **2014**, *6*, 1181−1197.
(32) Spencer, J.; Clarke, A. R.; Walsh, T. R. *J. Biol. Chem.* **2001**, *276*, 33638−33644.
(33) Rasia, R. M.; Vila, A. J. *J. Biol. Chem.* **2004**, *279*, 26046−26051.
(34) Xu, D.; Guo, H.; Cui, Q. *J. Am. Chem. Soc.* **2007**, *129*, 10814−10822.
(35) Park, H.; Brothers, E. N.; Merz, K. M., Jr. *J. Am. Chem. Soc. 2005* **2005**, *127*, 4232−4241.
(36) Dal Peraro, M.; Vila, A. J.; Carloni, P.; Klein, M. L. *J. Am. Chem. Soc.* **2007**, *129*, 2808−2816.
(37) Oelschlaeger, P.; Schmid, R. D.; Pleiss, J. *Protein Eng.* **2003**, *16*, 341−350.
(38) Dal Peraro, M.; Llarrull, L. I.; Rothlisberger, U.; Vila, A. J.; Carloni, P. *J. Am. Chem. Soc.* **2004**, *126*, 12661−12668.
(39) Rovira, C. *WIREs Comput. Mol. Sci.* **2013**, *3*, 393−407.
(40) Warshel, A.; Levitt, M. *J. Mol. Biol.* **1976**, *103*, 227−249.
(41) Marx, D.; Hutter, J.; *Ab Initio Molecular Dynamics: Basic Theory and Advanced Methods*; Cambridge University Press: Cambridge, 2009.
(42) Laio, A.; Parrinello, M. *Proc. Natl. Acad. Sci.* **2002**, *99*, 12562−12566.
(43) Iannuzzi, M.; Laio, A.; Parrinello, M. *Phys. Rev. Lett.* **2003**, *90*, 238302.
(44) Schaftenaar, G.; Noordik, J. H. *J. Comput.-Aided Mol. Design* **2000**, *14*, 123−134.
(45) Frisch, M. J., et al. *Gaussian 09, Revision B.01*; Gaussian, Inc.: Wallingford CT, 2010; see the Supporting Information for the complete reference.
(46) Cheatham, T. E.; Cieplak, P.; Kollman, P. A. *J. Biomol. Struct. Dyn.* **1999**, *16*, 845−62.
(47) Wang, J.; Wolf, R. M.; Caldwell, J. W.; Kollman, P. A.; Case, D. A. *J. Comput. Chem.* **2004**, *25*, 1157−1173.
(48) *RED: RESP ESP charge Derive*, Version III.3; see also http://q4md-forcefieldtools.org/RED/.
(49) Suárez, D.; Brothers, E. N.; Merz, K. M. *Biochemistry* **2002**, *41*, 6615−6630.
(50) Laio, A.; VandeVondele, J.; Rothlisberger, U. *J. Chem. Phys.* **2002**, *116*, 6941−6947.
(51) IBM Corp. *CPMD Program Package*, Version 13.2, 1990−2011; MPI für Festkörperforschung Stuttgart, 1997−2001; see also http://www.cpmd.org.
(52) Perdew, J. P.; Chevary, J. A.; Vosko, S. H.; Jackson, K. A.; Pederson, M. R.; Singh, D. J.; Fiolhais, C. *Phys. Rev. B* **1992**, *46*, 6671−6687.
(53) Vanderbilt, D. *Phys. Rev. B* **1990**, *41*, 7892−7895.
(54) Car, R.; Parrinello, M. *Phys. Rev. Lett.* **1985**, *55*, 2471−2474.
(55) Martyna, G. J.; Klein, M. L.; Tuckerman, M. *J. Chem. Phys.* **1992**, *97*, 2635−2643.
(56) Laio, A.; Parrinello, M. In *Computer Simulations in Condensed Matter: From Materials to Chemical Biology*; Ferrario, M., Cicotti, G., Binder, K., Eds.; Springer-Verlag: Berlin, Heidelberg, 2006; Vol. *1*, pp 315−347.
(57) Ensing, B.; Vivo, M. D.; Liu, Z.; Moore, P.; Klein, M. L. *Acc. Chem. Res.* **2006**, *39*, 73−81.
(58) Laio, A.; Gervasio, F. L. *Rep. Prog. Phys.* **2008**, *71*, 126601.
(59) Barducci, A.; Bonomi, M.; Parrinello, M. *WIREs Comput. Mol. Sci.* **2011**, *1*, 826−843.
(60) Tripathi, R.; Nair, N. N. *J. Am. Chem. Soc.* **2013**, *135*, 14679−14690.
(61) Kaminskaia, N. V.; Spingler, B.; Lippard, S. J. *J. Am. Chem. Soc.* **2000**, *122*, 6411−6422.
(62) Kaminskaia, N. V.; Spingler, B.; Lippard, S. J. *J. Am. Chem. Soc.* **2001**, *123*, 6555−6563.
(63) Crowder, M. W.; Spencer, J.; Vila, A. J. *Acc. Chem. Res.* **2006**, *39*, 721−728.
(64) Concha, N. O.; Janson, C. A.; Rowling, P.; Pearson, S.; Cheever, C. A.; Clarke, B. P.; Lewis, C.; Galleni, M.; Frère, J.-M.; Payne, D. J.; Bateson, J. H.; Abdel-Meguid, S. S. *Biochemistry* **2000**, *39*, 4288−4298.
(65) Leiros, H.-K. S.; Borra, P. S.; Brandsdal, B. O.; Edvardsen, K. S. W.; Spencer, J.; Walsh, T. R.; Samuelsenf, Ø. *Antimicrob. Agents Chemother.* **2012**, *56*, 4341−4353.
(66) Wu, S.; Xu, D.; Guo, H. *J. Am. Chem. Soc.* **2010**, *132*, 17986−17988.
(67) Spencer, J.; Read, J.; Sessions, R. B.; Howell, S.; Blackburn, G. M.; Gamblin, S. J. *J. Am. Chem. Soc.* **2005**, *127*, 14439−14444.
(68) Tioni, M. F.; Llarrull, L. I.; Poeylaut-Palena, A. A.; Martí, M. A.; Saggu, M.; Periyannan, G. R.; Mata, E. G.; Bennett, B.; Murgida, D. H.; Vila, A. J. *J. Am. Chem. Soc.* **2008**, *130*, 15852−15863.

DOI: 10.1021/acscatal.5b00242
ACS Catal. 2015, 5, 2577−2586